

Structure, electronic and electrochemical properties of Li-rich metal phosphate by first-principles study

Zhiping Lin¹, Yu-Jun Zhao², Yanming Zhao² and Jiantie Xu²

¹ School of Physics and Optoelectronic Engineering, Guangdong University of Technology, Guangzhou 510090, People's Republic of China

² Department of Physics, South China University of Technology, Guangzhou 510640, People's Republic of China

E-mail: zhipinglphy@gdut.edu.cn

Received 27 June 2013, revised 9 September 2013

Accepted for publication 16 September 2013

Published 11 December 2013

Abstract

We present a first-principles investigation for the structure, electronic properties, and average potentials of $\text{Li}_9\text{M}_3(\text{P}_2\text{O}_7)_3(\text{PO}_4)_2$ ($M = \text{V}, \text{Fe}, \text{Cr}$) compounds. The calculated Wyckoff coordinates are in good agreement with experimental observations. All the studied compounds show semiconductor characteristics, with band gaps between 1.89 eV and 2.55 eV. It is found that the Li-ion extraction is in the order of Li1(2b), Li2(12g), and Li3(4d) based on the calculated formation enthalpies of Li vacancies. Consequently, the calculated average potentials versus the number of Li ions are in good agreement with experiment.

Keywords: first-principles, monodiphosphates, Li-ion battery

(Some figures may appear in colour only in the online journal)

1. Introduction

In recent years, the phosphates of systems $\text{A}_2\text{O}-\text{M}_2\text{O}_3-\text{P}_2\text{O}_5$ have been extensively studied due to their fast A^+ ion transport properties, such as the Nasicon-type monophosphates $\text{A}_3\text{Fe}_2(\text{PO}_4)_3$ [1, 2], the monoclinic $\beta\text{-Fe}_2(\text{SO}_4)_3$ -type modification of $\text{Li}_3\text{Fe}_2(\text{PO}_4)_3$ [3], the monodiphosphates $\text{Na}_7(\text{MP}_2\text{O}_7)_4\text{PO}_4$ [4] and the diphosphates $\text{Na}_7\text{M}_3(\text{P}_2\text{O}_7)_4$ [5]. Polyanions build 3D structures by PO_4 tetrahedra and MO_6 octahedra, which are of interest for potential application as positive electrodes for lithium rechargeable batteries. Efforts have focused on $\text{Li}_3\text{Fe}_2(\text{PO}_4)_3$ [6, 7] and $\text{Li}_3\text{V}_2(\text{PO}_4)_3$ [8–10]. Monoclinic $\text{Li}_3\text{V}_2(\text{PO}_4)_3$ contains both removable Li cations and redox-active metal sites housed within a rigid phosphate framework. Barker [11] *et al* and Sato [12] *et al* have reported that lithium can extract out of the structure and form a potential >4.6 eV when the last type of lithium is extracted. Unlike the rhombohedral phase, the monoclinic phase [13, 14] is thermodynamically more stable and displays a complex series of two-phase transitions on Li extraction and a solid solution region on Li reinsertion. Yin *et al* [8] investigated the correlation of the structural features in the series of single-phase materials $\text{Li}_{3-y}\text{V}_2(\text{PO}_4)_3$

with the electrochemical voltage-composition profile and mainly highlighted the importance of ion-ion interactions in determining phase transitions. The experimental results [9, 10] also indicate that the carbon-coating can enhance the electrode reaction reversibility and the capacity retention and rate performance.

The layered monodiphosphates with trigonal space group $P-3c1$, $\text{Li}_9\text{M}_3(\text{P}_2\text{O}_7)_3(\text{PO}_4)_2$, were firstly synthesized by flux method from $\text{A}_2\text{O}-\text{M}_2\text{O}_3-\text{P}_2\text{O}_5$ systems [15]. The structure consists of $\infty^2[(\text{MP}_2\text{O}_7)_3(\text{PO}_4)_2]^{9-}$ corrugated layers that are parallel to (001) and separated by lithium ions, as shown in figure 1. The $\infty^2[(\text{MP}_2\text{O}_7)_3(\text{PO}_4)_2]^{9-}$ layers are built up of MO_6 octahedra sharing corners with PO_4 tetrahedra and P_2O_7 groups. It has been confirmed that lithium can extract off the $\text{Li}_9\text{M}_3(\text{P}_2\text{O}_7)_3(\text{PO}_4)_2$ ($M = \text{V}, \text{Fe}, \text{Cr}$) structure and lead to a voltage potential of 3–4.9 V [16–19]. The results of $\text{Li}_x\text{V}_3(\text{P}_2\text{O}_7)_3(\text{PO}_4)_2$ [16, 17] display that about 82% (142 mAh g^{-1}) of the theoretical capacity (173 mAh g^{-1}) is attainable on the first oxidation cycle. On discharge, most Li ($\sim 96\%$) can be re-inserted, and the reversible capacities are located in between ~ 142 and 136 mAh g^{-1} . However, studies of the ferrated and cobaltic compounds are very rare. Though $\text{Li}_9\text{Fe}_3(\text{P}_2\text{O}_7)_3(\text{PO}_4)_2$ has been synthesized by our group,

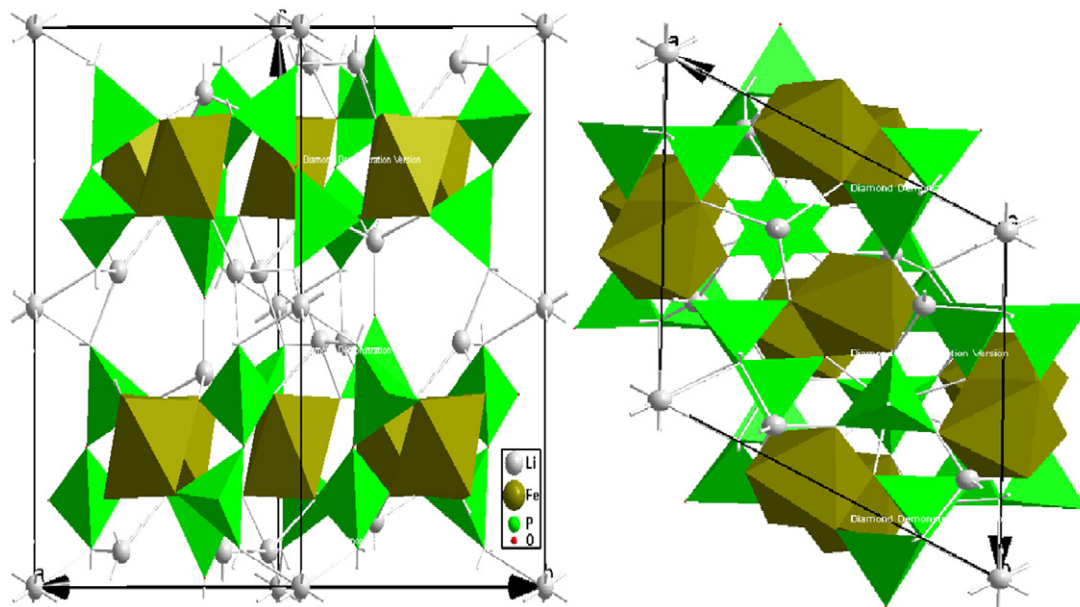


Figure 1. Structure of $\text{Li}_9\text{M}_3(\text{P}_2\text{O}_7)_3(\text{PO}_4)_2$ ($M = \text{V}, \text{Fe}, \text{Cr}, \text{Co}$).

$\text{Li}_9\text{Co}_3(\text{P}_2\text{O}_7)_3(\text{PO}_4)_2$ has not been reported to date. In this paper, based on first-principles calculation with the Hubbard term corrected general gradient approximation (GGA+U), we investigated the structure, electronic properties and average potentials of $\text{Li}_9\text{M}_3(\text{P}_2\text{O}_7)_3(\text{PO}_4)_2$ ($M = \text{V}, \text{Fe}, \text{Co}, \text{Cr}$). Conductivity of compounds is obtained by investigating the electronic structure and the band gap. Based on the calculation of the formation enthalpy of Li vacancy, the order of Li-ion extraction is obtained and average potentials versus the number of Li ions is calculated, with a comparison to the corresponding experiment.

2. Computational details

The calculations are based on density-functional theory with the general gradient approximation using PW91 form for the exchange correlation energy [20] as implemented in the Vienna Ab-Initio Simulation Package (VASP) [21], plus the Hubbard term correction (GGA+U) to give a better description on the strong correlation of transition metal oxides. The unit cells of the relevant structures may contain up to 98 ions making the computations particularly demanding. The interactions between valence electrons and ions were represented with the projector augmented wave (PAW) pseudo-potentials. The numbers of atoms considered are 9, 3, 8 and 29 for Li, V, P and O atoms, respectively. The structure was fully relaxed with respect to internal and external cell parameters and atomic position using forces and stresses. The wave functions were expanded in plane waves with an energy cutoff of 400 eV. Brillouin zone integration of the total energies was performed with a $3 \times 3 \times 2$ Monkhorst–Pack mesh and the total energies were converged within 10^{-3} eV with respect to k -points. Fermi level is smeared by the Gaussian method with a width of 0.1 eV. The average insertion voltage is given by $\bar{V} = -(\Delta G_r/F)$, where F is the Faraday constant.

3. Results and discussion

3.1. Structural properties

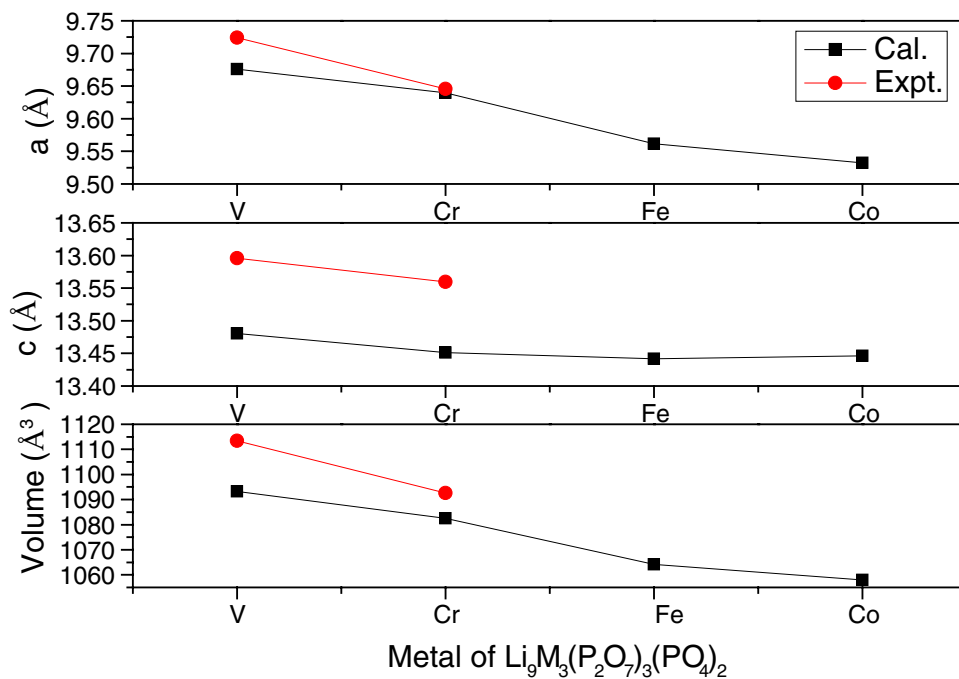
$\text{Li}_9\text{M}_3(\text{P}_2\text{O}_7)_3(\text{PO}_4)_2$ is a hexagonal structure with the symmetry group $P-3c1$, which is composed of MO_6 octahedra sharing corners with monophosphate tetrahedral PO_4 and diphosphate groups P_2O_7 . Each unit cell contains two chemical formula units. Calculated atomic coordinates of $\text{Li}_9\text{M}_3(\text{P}_2\text{O}_7)_3(\text{PO}_4)_2$ ($M = \text{V}, \text{Fe}, \text{and Co}$) are listed in table 1. Computed Wyckoff coordinates are in good agreement with experimental values. Calculated ferrated and cobaltic atomic coordinates are basically in agreement with that of $\text{Li}_9\text{V}_3(\text{P}_2\text{O}_7)_3(\text{PO}_4)_2$ structure, as the changes are due to the difference of metal ion radius. Calculated crystal parameters and volume of $\text{Li}_9\text{M}_3(\text{P}_2\text{O}_7)_3(\text{PO}_4)_2$ ($M = \text{Fe}, \text{Cr}, \text{Co}, \text{V}$) are also shown in figure 2. It displays that calculated values are smaller than the corresponding experimental values by 1.6%. It can be seen that the lattice parameter a and volume V decrease from V to Co compound, which is in accordance with the corresponding atomic radii. Interestingly, the tendency of the lattice parameter c is different, as the lattice parameter c of Co compound is larger than that of Fe compound.

3.2. Electronic properties

The analysis of the electronic structure often reflects the conductivity of the cathode materials. The GGA+U approach usually improves the treatment of correlation effects in localized orbitals that are formed by the metal 3d orbital and oxygen 2p hybridization. In GGA+U, local atoms like 3d states are projected out and treated with a Hubbard model. Therefore, this method makes more applicable to transition metal compound to correct the energies and to improve the band structures and magnetic moments. For example, in the case of LiFePO_4 the calculated band gap from GGA lies in the range of 0–0.3 eV, but the GGA+U

Table 1. Calculated Wyckoff coordinates of $\text{Li}_9\text{M}_3(\text{P}_2\text{O}_7)_3(\text{PO}_4)_2$ ($M = \text{V}, \text{Fe}, \text{Cr}$), compared with experimental values (in parentheses) [16].

Atoms	Wyckoff sites	$\text{Li}_9\text{V}_3(\text{P}_2\text{O}_7)_3(\text{PO}_4)_2$ (Expt.)	$\text{Li}_9\text{Fe}_3(\text{P}_2\text{O}_7)_3(\text{PO}_4)_2$	$\text{Li}_9\text{Co}_3(\text{P}_2\text{O}_7)_3(\text{PO}_4)_2$
P1	4d	(0.6666, 0.3333, 0.6228) (2/3, 1/3, 0.6264)	(0.6666, 0.3332, 0.6281)	(0.6666, 0.3333, 0.6277)
P2	12g	(0.3146, 0.0877, 0.8462) (0.3163, 0.0894, 0.8450)	(0.3185, 0.0899, 0.8448)	(0.3197, 0.0909, 0.8441)
Fe	6f	(0.5692, 0, 3/4) (0.5668, 0, 3/4)	(0.5685, 0, 0.75)	(0.5681, 0, 0.75)
Li1	2b	(0, 0, 0) (0, 0, 0)	(0, 0, 0)	(0, 0, 0)
Li2	4d	(0.6667, 0.3334, 0.8752) (2/3, 1/3, 0.8840)	(0.6667, 0.3332, 0.8776)	(0.6667, 0.3333, 0.8776)
Li3	12g	(0.3377, 0.0997, 0.0615) (0.3362, 0.1036, 0.0644)	(0.3389, 0.1001, 0.0625)	(0.3390, 0.1003, 0.0622)
O1	4d	(0.6667, 0.3333, 0.5108) (2/3, 1/3, 0.5156)	(0.6667, 0.3333, 0.5152)	(0.6667, 0.3333, 0.5147)
O2	6f	(0.2089, 0, 3/4) (0.2120, 0, 3/4)	(0.2089, 0, 0.75)	(0.2089, 0, 0.75)
O3	12g	(0.6795, 0.1893, 0.6633) (0.6743, 0.1863, 0.6635)	(0.6803, 0.1874, 0.6673)	(0.6811, 0.1867, 0.6658)
O4	12g	(0.4814, 0.1069, 0.8348) (0.4796, 0.1054, 0.8365)	(0.4858, 0.1057, 0.8340)	(0.4878, 0.1072, 0.8332)
O5	12g	(0.3284, 0.2523, 0.8476) (0.3291, 0.2537, 0.8440)	(0.3343, 0.2575, 0.8456)	(0.3351, 0.2590, 0.8449)
O6	12g	(0.2222, -0.0082, 0.9364) (0.2228, -0.0045, 0.9353)	(0.2247, -0.0037, 0.9361)	(0.2255, -0.0017, 0.9358)

**Figure 2.** Calculated crystal parameters and voltages of $\text{Li}_9\text{M}_3(\text{P}_2\text{O}_7)_3(\text{PO}_4)_2$ ($M = \text{Fe}, \text{Cr}, \text{Co}, \text{V}$), with experimental values [16, 19] displayed in red.

result is about 3.7 eV, close to the measured value from diffuse reflectance spectroscopy [19]. The electronic density of states (DOS) are shown in figure 3 for $\text{Li}_9\text{M}_3(\text{P}_2\text{O}_7)_3(\text{PO}_4)_2$, where the behaviour of the band around the Fermi level is dominated by the d-states of transition metal, and the band width around the Fermi level is formed by the hybridization of the Li s-states and p-states, oxygen p-states, and the transition metal d-states. All materials show semiconductor

characteristics. The width of band gap is 1.89 eV (figure 3(a)) for $\text{Li}_9\text{Co}_3(\text{P}_2\text{O}_7)_3(\text{PO}_4)_2$, 2.15 eV for $\text{Li}_9\text{V}_3(\text{P}_2\text{O}_7)_3(\text{PO}_4)_2$ (figure 3(b)), 2.11 eV for $\text{Li}_9\text{Fe}_3(\text{P}_2\text{O}_7)_3(\text{PO}_4)_2$ (figure 3(c)), and 2.55 eV for $\text{Li}_9\text{Cr}_3(\text{P}_2\text{O}_7)_3(\text{PO}_4)_2$ (figure 3(d)). The band gap of $\text{Li}_9\text{Cr}_3(\text{P}_2\text{O}_7)_3(\text{PO}_4)_2$ is the widest and that of $\text{Li}_9\text{Co}_3(\text{P}_2\text{O}_7)_3(\text{PO}_4)_2$ is the shallowest. The calculated semiconductor characteristic of these compounds is in

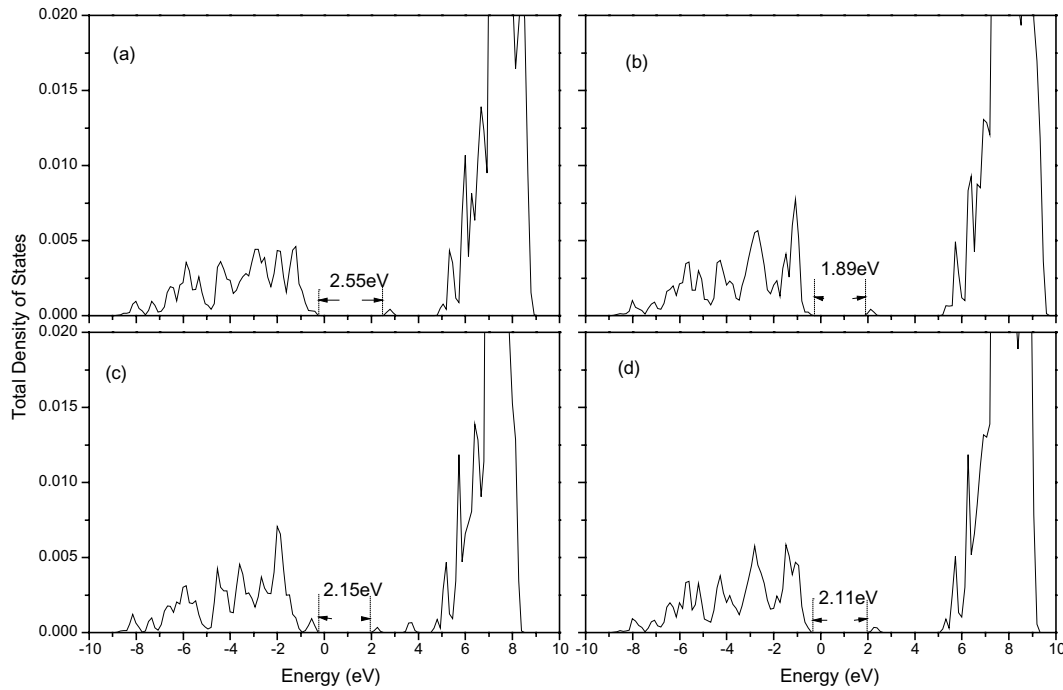


Figure 3. Total density of states for $\text{Li}_9\text{M}_3(\text{P}_2\text{O}_7)_3(\text{PO}_4)_2$. (a) $\text{Li}_9\text{Cr}_3(\text{P}_2\text{O}_7)_3(\text{PO}_4)_2$ with $U = 3.5$; (b) $\text{Li}_9\text{Co}_3(\text{P}_2\text{O}_7)_3(\text{PO}_4)_2$ with $U = 5.0$; (c) $\text{Li}_9\text{V}_3(\text{P}_2\text{O}_7)_3(\text{PO}_4)_2$ with $U = 4.0$; (d) $\text{Li}_9\text{Fe}_3(\text{P}_2\text{O}_7)_3(\text{PO}_4)_2$ with $U = 4.5$.

good agreement with the experimental result of electronic conductivity measurement [17].

3.3. Extraction order of Li-ion

When Li is extracted from the structure, it creates a Li vacancy at its original position. Due to Li atoms located in three different Wyckoff sites, Li1(2b), Li2(4d) and Li3(12g), and thus there are three types of Li vacancy in this compound. The formation enthalpy of Li vacancy with the zero charge state is determined by $\Delta tH^{(V_{\text{Li}})} = E(V_{\text{Li}}) - E(0) + \mu_i^{\text{element}}$, where $E(V_{\text{Li}})$ and $E(0)$ are the total energy of the cell with and without a vacancy V_{Li} . Our calculations show that the formation enthalpy of Li1 vacancy is lower by 0.735 eV and 0.489 eV than that of Li2 and Li3 vacancies, respectively, and then lithium ions in Li1 site are the first extracted at the lowest voltage. Comparing the formation enthalpies of Li2 and Li3 vacancies, it can be seen that the formation of Li3 vacancy is easier than that of Li2 vacancy. Therefore, based on our first-principles calculation results, Li-ion extraction is in the sequence of Li1, Li3, and Li2 in $\text{Li}_x\text{M}_3(\text{P}_2\text{O}_7)_3(\text{PO}_4)_2$, in agreement with the symmetry of $P\bar{3}c1$ space group.

3.4. The average potentials versus the number of Li ions per formula

Base on this extraction sequence of Li ions (Li(1) \rightarrow Li(3) \rightarrow Li(2)), we have calculated the average potentials versus the number of Li ions per formula through obtained total energy of $\text{Li}_x\text{V}_3(\text{P}_2\text{O}_7)_3(\text{PO}_4)_2$ ($x = 8, 6, 3$). Based on this extraction sequence, we also calculated the average potentials versus the number of Li ions per formula through the total energy of $\text{Li}_x\text{M}_3(\text{P}_2\text{O}_7)_3(\text{PO}_4)_2$ ($M = \text{Co}, \text{Cr}$ and

Fe) ($x = 8$). The results are shown in figure 4, which are compared with available experimental values [16–19]. It can be seen that the calculated results are basically in agreement with the main characteristic of the experimental values. For $\text{Li}_x\text{V}_3(\text{P}_2\text{O}_7)_3(\text{PO}_4)_2$ [16, 17], the first voltage plateau at 3.40 V is lower than the experimental value of 3.75 V, and the second and third plateaus are in good agreement with the experimental result. The difference between experimental and computational results may be due to the lack of consideration on the two-phase reaction effect. For $\text{Li}_x\text{M}_3(\text{P}_2\text{O}_7)_3(\text{PO}_4)_2$ ($M = \text{Fe}, \text{Cr}$) ($x = 8$) compounds, the calculated average potentials versus the number of Li ions per formula is about 4.6 V, which is slightly lower than experimental results. Of note, $\text{Li}_9\text{Co}_3(\text{P}_2\text{O}_7)_3(\text{PO}_4)_2$ compound has not been synthesized up to now. The calculated average potentials, which are similar to the Li-ion extraction sequence of the $\text{Li}_9\text{V}_3(\text{P}_2\text{O}_7)_3(\text{PO}_4)_2$, indicate that the first-oxidation process occurs approximately on 3.74 V voltage. The second-oxidation process is above 4.8 V voltage, which is higher than that of the $\text{Li}_9\text{V}_3(\text{P}_2\text{O}_7)_3(\text{PO}_4)_2$. Along with more Li ions extraction the voltage plateau of the $\text{Li}_9\text{Co}_3(\text{P}_2\text{O}_7)_3(\text{PO}_4)_2$ materials will overrun 5 V voltage, which is beyond the safe limit of the used 1M LiPF₂ in EC:DMC (1:1 vol%) electrolyte system. Hence, under common used electrolyte the reversible capacity of $\text{Li}_9\text{Co}_3(\text{P}_2\text{O}_7)_3(\text{PO}_4)_2$ is less than 100 mAh g⁻¹, which is not available on the commercial cathode material of Li-ion batteries.

Table 2 lists the change of volume and lattice parameters with different Li-ion numbers. It can be seen that the calculated volume and lattice parameters are less than the experimental result. Along with the first Li-ion extraction, the lattice structure has not changed remarkably. When more Li-ions are going on extraction from materials (for example

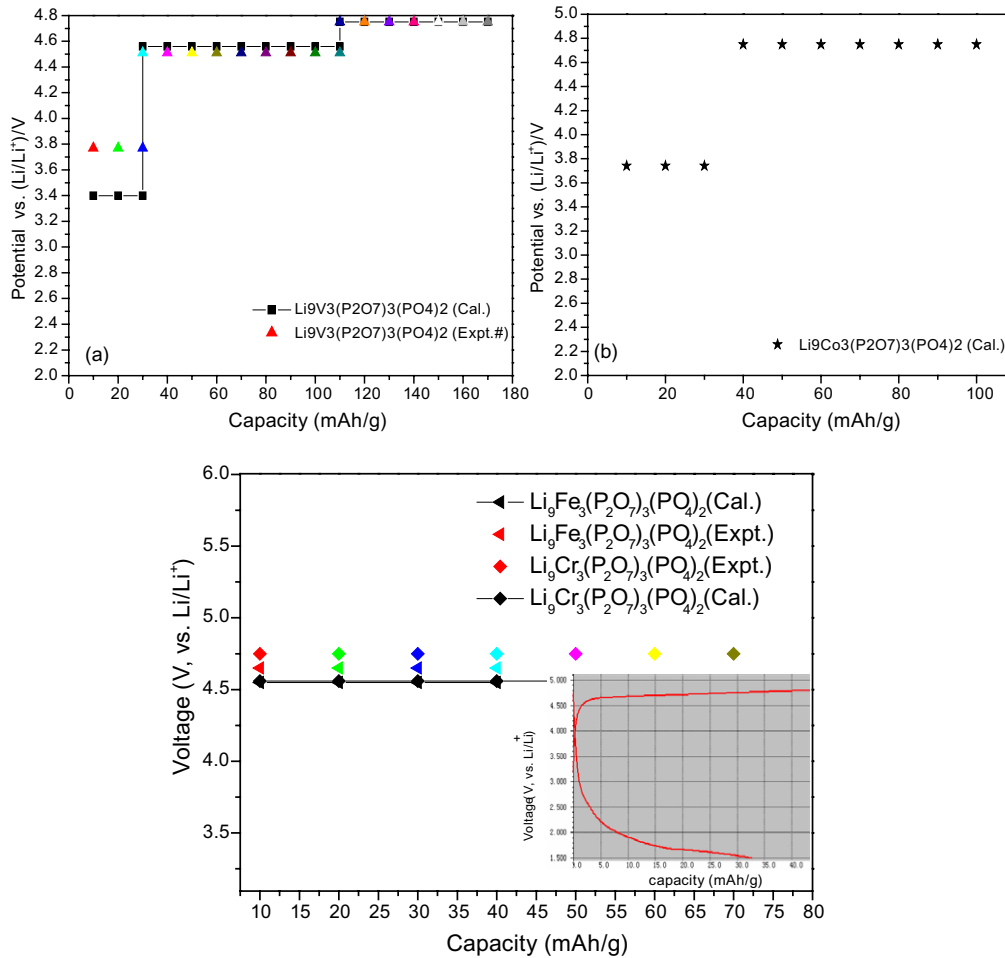


Figure 4. The charge and discharge profile of $\text{Li}_9\text{M}_3(\text{P}_2\text{O}_7)_3(\text{PO}_4)_2$ ($M = \text{V}, \text{Fe}, \text{Co}$ and Cr) by first-principles calculation, along with the experimental values [16–19]. The charge and discharge curve of $\text{Li}_9\text{Fe}_3(\text{P}_2\text{O}_7)_3(\text{PO}_4)_2$ is shown in the insert figure of figure 6(c) [22].

Table 2. Lattice parameters and volume change of $\text{Li}_9\text{M}_3(\text{P}_2\text{O}_7)_3(\text{PO}_4)_2$ ($M = \text{Fe}, \text{Co}, \text{V}$) along with Li-ion extraction, and experimental results are listed in parentheses.

M	V					
	The number of extract ions	Fe 1	Co 1	1	3	6
a (Å)		9.5407 (9.5615)	9.5113 (9.5321)	9.6680 (9.6761)	9.6275	9.5565
c (Å)		13.4216 (13.4416)	13.4523 (13.4462)	13.4674 (13.4806)	13.4407	13.1714
β , γ		90	90	90	90.15, 90.04	90.10, 90.02
V		1058.02 (1064.23)	1054.01 (1058.04)	1090.12 (1093.21)	1078.00	1041.66

$\text{Li}_x\text{V}_3(\text{P}_2\text{O}_7)_3(\text{PO}_4)_2$, $x < 6$), the angle β appears to change, resulting in the change of the symmetry of space group during insertion/deinsertion of Li ions. The experiment result [16–18] has discovered that the second phase of C3 sample has a similar parameter a (9.439 Å) to the first phase (9.812 Å) and parameter b (27.245 Å) of almost double the first one (13.598 Å). The trigonal lattice of the second phase can be regarded as the supercell of two original lattices along c axis.

Our calculation can also find that the supercell energy of phase is greater than that of single phase. Thus, the supercell structure phase is considered to only exist as a metal-stable state at high potential and can easily be transited to $P\bar{3}c1$ space symmetry during discharge. Along with more Li extraction, V ions of low valence state have been oxidized to that of high valence state with smaller ionic radii (for example: V^{3+} : 0.78 Å, V^{4+} : 0.72 Å, and V^{5+} : 0.68 Å) [22], which can lead to the shrink of a and b axes. The remaining Li ions can sustain the layered structure and no distinct contraction is displayed along c axis, which can benefit the reinsertion of Li ions during discharge. The volume change of $\text{Li}_9\text{V}_3(\text{P}_2\text{O}_7)_3(\text{PO}_4)_2$ is 4.49% (Expt [17]. $\sim 1.16\%$) that is smaller than that of $\text{Li}_3\text{V}_2(\text{PO}_4)_3$ (Expt [8]. 6.87%) when six lithium ions extract from the compounds. Therefore, this small volume change is very beneficial to improve the retention rate of discharge capacity, and this material is used as cathode of lithium ion battery.

4. Conclusion

We present a first-principles calculation for the structure, electronic properties and average potentials of $\text{Li}_9\text{M}_3(\text{P}_2\text{O}_7)_3(\text{PO}_4)_2$ ($M = \text{V}, \text{Fe}, \text{Cr}$) compounds. The

calculation is based on density-functional theory with the general gradient approximation GGA+U. The results of calculated Wyckoff coordinates are in good agreement with experimental values. All materials show semiconductor characteristics, with the width of band gap between 1.89 and 2.55 eV. Along with the obtained formation enthalpies of Li(1), Li(2) and Li(3) vacancies, the Li-ion extraction is in proper order of Li(1), Li(3), and Li(2), in agreement with the symmetry of $P\bar{3}c1$ space group. Base on this extraction sequence (Li(1) \rightarrow Li(3) \rightarrow Li(2)), Calculated average potentials versus the number of Li ions is between 3.4 V and 4.9 V, which is in good agreement with available experiment.

Acknowledgments

This work was funded by NSFC Grant (Nos 11204042, 51172077 and 11174082) through NSFC Committee of China and the Foundation (No S2011020000521) through the Science and Technology Bureau of Guangdong Government, respectively.

References

- [1] d'Yvoire F, Pintard-Scrépel M, Bretey E and de Ia Rochère M 1983 *Solid State Ion.* **9** 851
- [2] Lyutin I S, Melnikov O K, Sigaryov S E and Terziev V G 1988 *Solid State Ion.* **31** 197
- [3] Ivannov-Shits A K and Schoonman J 1996 *Solid State Ion.* **91** 93
- [4] Masquelier C, d'Yvoire F and Rodier N 1991 *J. Solid State Chem.* **95** 156
- [5] Masquelier C, d'Yvoire F, Bretey E, Berthet P and Prytour-Chansac C 1994 *Solid State Ion.* **67** 183
- [6] Padhi A K, Nanjundaswamy K S, Masquelier C and Goodenough J B 1997 *J. Electrochem. Soc.* **144** 2581
- [7] Masquelier C, Padhi A K, Nanjundaswamy K S and Goodenough J B 1998 *J. Solid State Chem.* **135** 228
- [8] Yin S-C, Grondey H, Strobel P, Anne M and Nazar L F 2003 *J. Am. Chem. Soc.* **125** 10402
- [9] Fu P, Zhao Y M, An X N, Dong Y Z and Hou X M 2007 *Electrochem. Acta* **52** 5281
- [10] Fu P, Zhao Y M, Dong Y Z, An X N and Shen G P 2006 *J. Power Sources* **162** 651
- [11] Barker J and Saidi M Y 2001 *US Patent* 6, 203,946
- [12] Sato M, Ohkawa H, Yoshida K, Saito M, Uematsu K and Toda K 2000 *Solid State Ion.* **135** 137
- [13] Huang H, Yin S-C, Kerr Y and Nazar L F 2002 *Adv. Mater.* **14** 1525
- [14] Ohkawa H, Yoshida K, Saito M, Uematsu K, Toda K and Sato M 1999 *Chem. Lett.* 1017
- [15] Poisson S, d'Yvoire F, Nguyen-Huy-Dung, Bretey E and Berthet P 1998 *J. Solid State Chem.* **138** 32
- [16] Quan K, Xu J T, Zhao Y M, Chen X L and Chen L Q 2011 *Electrochim. Acta* **56** 2201
- [17] Quan K, Lin Z P, Zhao Y M, Chen X L and Chen L Q 2011 *J. Mater. Chem.* **21** 14760
- [18] Quan K, Zhao Y M and Xu J T 2011 *J. Phys. Chem. C* **115** 8422
- [19] Xu J T and Zhao Y M 2011 *J. Sol-Gel Sci. Technol.* **59** 521
- [20] Perdew J P et al *Phys. Rev. B* **46** 6671
- [21] Kresse G and Hafner J 1993 *Phys. Rev. B* **47** 558
- [21] Kresse G and Hafner J 1994 *Phys. Rev. B* **49** 14251
- [21] Kresse G and Furthmuller J 1996 *Comput. Mater. Sci.* **6** 15
- [21] Kresse G and Furthmuller 1996 *Phys. Rev. B* **54** 11169
- [22] Xu J T 2012 *Thesis of Master Degree*